



HAL
open science

Decay of semi-diurnal internal-tide beams due to subharmonic resonance

Theo Gerkema, Chantal Staquet, Pascale Bouruet-Aubertot

► **To cite this version:**

Theo Gerkema, Chantal Staquet, Pascale Bouruet-Aubertot. Decay of semi-diurnal internal-tide beams due to subharmonic resonance. *Geophysical Research Letters*, 2006, 33 (8), pp.L08604. 10.1029/2005GL025105 . hal-00264654

HAL Id: hal-00264654

<https://hal.science/hal-00264654>

Submitted on 19 Jul 2021

HAL is a multi-disciplinary open access archive for the deposit and dissemination of scientific research documents, whether they are published or not. The documents may come from teaching and research institutions in France or abroad, or from public or private research centers.

L'archive ouverte pluridisciplinaire **HAL**, est destinée au dépôt et à la diffusion de documents scientifiques de niveau recherche, publiés ou non, émanant des établissements d'enseignement et de recherche français ou étrangers, des laboratoires publics ou privés.

Copyright

Decay of semi-diurnal internal-tide beams due to subharmonic resonance

Theo Gerkema,¹ Chantal Staquet,² and Pascale Bouruet-Aubertot³

Received 1 November 2005; revised 20 January 2006; accepted 20 March 2006; published 21 April 2006.

[1] Results of a numerical study on internal-tide generation are presented, using the nonlinear nonhydrostatic MIT-GCM. In the model runs, a lunar semidiurnal (M2) internal tide beam is generated over the continental shelf break. Its further nonlinear evolution is analysed, in particular the generation of M1 internal tides by Subharmonic Resonance (SR). This is done for three different latitudes: at a mid-latitude, slightly below (i.e., equatorward of) the critical latitude (poleward of which the M1 internal tide cannot propagate as a free wave), and at the equator. In the second case the M2 beam loses much energy to M1 already over the continental slope, yielding a pronounced spectral peak at M1, as well as a distinct M1 signal in the current velocity field. At the equator, the transfer to M1 is less pronounced, but still noticeable. Analysis of the growth rate of M1 yields a timescale of two days. **Citation:** Gerkema, T., C. Staquet, and P. Bouruet-Aubertot (2006), Decay of semi-diurnal internal-tide beams due to subharmonic resonance, *Geophys. Res. Lett.*, *33*, L08604, doi:10.1029/2005GL025105.

1. Introduction

[2] Direct and indirect evidence of energy transfer from the lunar semi-diurnal internal-tide (M2) to its subharmonic ($\frac{1}{2}$ M2, hereafter denoted as M1) has been gathered in recent years. This process occurs through Subharmonic Resonance (SR), also called Parametric Subharmonic Instability (PSI). SR can take place equatorward of the ‘critical’ latitude 28.8°N/S , because in the meridional band $28.8^\circ\text{S}–28.8^\circ\text{N}$ the M1-frequency exceeds the (absolute) local Coriolis parameter, $|f|$, allowing the M1 internal tide to propagate as a free internal wave.

[3] In observations at Kaene Ridge (Oahu, near 22°N), *Carter and Gregg* [2006] find a strong signal at the diurnal frequency, just above the local inertial frequency. Although the time-series is too short to distinguish an M1 spectral peak from those at other diurnal frequencies (such as K1, O1), a bicoherence analysis shows that the diurnal and semidiurnal signals are nonlinearly coupled. Hence the interpretation, put forward by *Carter and Gregg* [2006], that the diurnal peak represents M1, at least in part, and can be ascribed to SR. This would imply that the transfer from M2 to M1 occurs already very close to the region where the M2 internal tide itself is generated, within a distance of

35 km. Our numerical results, presented below, support this idea.

[4] Previous numerical experiments already demonstrated that a transfer from a mode-1 M2 internal-tide to its subharmonic can take place [*Hibiya et al.*, 2002]; moreover, this transfer was recently shown to be particularly strong just below the critical latitude 28.8°N [*MacKinnon and Winters*, 2005].

[5] Finally, accumulating indirect evidence is presented by *Nagasawa et al.* [2002] and *Hibiya and Nagasawa* [2004], who used expendable current profilers to show that fine-scale shear and diapycnal diffusivity are generally enhanced equatorward of about 30°N ; they put forward the interpretation that this is due to the generation, by SR, of M1 internal tides with high vertical wavenumber.

[6] The principal goal of this paper is to identify, in a numerical study, at which stage of its ‘life’ the M2 internal tide starts suffering from SR. For this purpose, we start from the very origin of the internal tide (rather than from a pre-imposed internal-tide field, as in the above-mentioned numerical studies), in this case its generation over the continental slope. For comparison, we consider three latitudes: 45°N (mid-latitude), 27.5°N (just below the critical latitude), and 0°N (equator).

[7] The established picture is that a downward propagating beam is generated near the shelf edge, and later reflects at the bottom of the deep ocean [e.g., *Pingree and New*, 1991]. This is what we will find here too, but the question is whether SR starts to act before or after bottom reflection. During bottom reflection the M2 beam generates higher harmonics (M4, M6 etc.), thereby losing energy [*Gerkema et al.*, 2006], which leaves less energy for SR. It would thus seem that for SR to gain much significance, it should be at work at an early stage, i.e., before bottom reflection. In this respect, the time-scale estimated by *MacKinnon and Winters* [2005], 5 days, although shorter than previous estimates, would still be too long. The observations by *Carter and Gregg* [2006] point however to a shorter time-scale (given the proximity to the generation region), and this will be confirmed in a different and somewhat idealized setting of our model runs, carried out for three latitudes.

2. Model

[8] We use the nonlinear nonhydrostatic MIT-GCM [*Marshall et al.*, 1997] in an essentially 2D setting, that is, we assume uniformity in the along-slope direction, while allowing a Coriolis-induced along-slope current to exist. The forcing by the M2 barotropic tide is prescribed by imposing a cross-slope barotropic flow at the boundaries, giving a time-oscillatory but spatially constant barotropic flux. A sponge-layer is added at the lateral boundary of the

¹Royal Netherlands Institute for Sea Research, Texel, Netherlands.

²Laboratoire des Ecoulements Géophysiques et Industriels, Grenoble, France.

³Laboratoire d’Océanographie et du Climat: Expérimentation et Approches Numériques, IPSL, Paris, France.

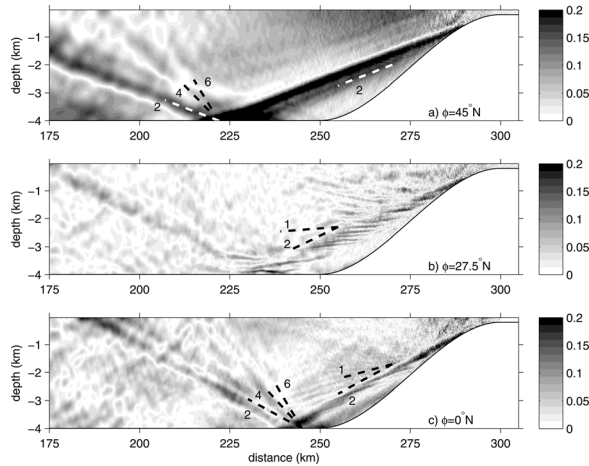


Figure 1. The absolute value of the cross-slope baroclinic current, after 15 (M2) tidal periods, at three different latitudes. Dashed lines indicate the directions of energy propagation, according to (1); here ‘1’ refers to M1, ‘2’ to ‘M2’ etc.

deep ocean to absorb the baroclinic waves [Gerkema *et al.*, 2006].

[9] The parameters are chosen as follows. The initial temperature field is chosen such that the buoyancy frequency is uniform: $N = 2 \times 10^{-3}$ rad/s. The forcing is at the M2 tidal frequency $\sigma_{M2} = 1.405 \times 10^{-4}$ rad/s, with a barotropic cross-slope tidal flux of $100 \text{ m}^2/\text{s}$. These are values typical of continental-slope regions where significant internal-tide generation takes place [cf., Gerkema *et al.*, 2004]. The continental slope has a length of 50 km and is described by a cubic polynomial; it represents the transition from the deep ocean (waterdepth 4 km) to the continental shelf (waterdepth 200 m). In the cross-slope direction 4000 cells of 100 m are used, and in the vertical 160 cells of 25 m (in the deepest part), making the domain 400 km by 4 km. The time step is 11.179s (4000 time steps per tidal period). An implicit free surface is used. Vertical diffusivity and viscosity are each $10^{-4} \text{ m}^2/\text{s}$; the horizontal ones are $10^{-2} \text{ m}^2/\text{s}$.

[10] We consider three latitudes: 45°N (mid-latitude, $f = 1.0 \times 10^{-4}$ rad/s), 27.5°N (just below the critical latitude, $f = 6.73 \times 10^{-5}$ rad/s), and 0°N (equator, $f = 0$). In each case, the run spans 15 M2 tidal periods.

3. Results

[11] Figure 1 shows the cross-slope horizontal velocity component at the final moment of the run, i.e., after 15 M2 tidal periods. At this instant, the barotropic tidal current is zero, so the field shown here is purely baroclinic. In each case, an internal tide beam is seen to emanate from the upper part of the slope. Its steepness is different in different panels, because of the dependence on the Coriolis parameter f . In linear theory, this steepness γ is given by

$$\gamma^2 = \frac{\sigma^2 - f^2}{N^2 - \sigma^2} \quad (1)$$

[e.g., LeBlond and Mysak, 1978]. In Figures 1a–1c, dashed lines based on this expression are added for a choice of

frequencies as appropriate; this includes the M2 internal tide itself (frequency σ_{M2}), its subharmonic M1 ($\frac{1}{2}\sigma_{M2}$), and its higher harmonics M4 ($2\sigma_{M2}$) and M6 ($3\sigma_{M2}$). Steepness γ in (1) is a monotonically increasing function of σ ; the subharmonic is thus less steep than the M2 beam, while the higher harmonics are steeper. Higher harmonics are mainly generated when the beam reflects at the bottom, due to interaction between the incoming and outgoing beams [Tabaei *et al.*, 2005]. In Figures 1a–1c, a ‘fountain’ of higher harmonics is discernible which originates from the region of bottom reflection (near $x = 220, 230,$ and 240 km, respectively). The spectra, discussed below, show this more clearly and quantitatively.

[12] We note that the mere change of the Coriolis parameter f , the only difference between Figures 1a–1c, changes a number of things at once: the direction of the M2 beam – an immediate consequence of (1); the location of most effective generation of M2 internal-tide beams, because the point of critical reflection lies higher up the slope for higher f ; and the width and intensity of the beam, which in turn affects subsequent nonlinear processes.

[13] In Figure 1b we see that the main beam is intersected by near-horizontal ‘slices’ whose direction corresponds to that of M1; the slices can thus be interpreted as troughs and crests of M1 beams. They appear already within a distance of 10 km of the generation region, implying that the M2 beam starts to suffer from SR almost immediately after its generation. This supports the interpretation of the observational findings by Carter and Gregg [2006], which were made at a somewhat lower latitude. At the equator, too, one observes ‘slices’ that correspond to the theoretically predicted direction of M1 beams (Figure 1c). This shows that SR occurs even at the equator, although the effect is weaker there than at 27.5°N .

[14] The M1 signal, already visible in Figure 1b, is brought out more clearly by multiplying the u -component by $\cos(\sigma_{M1}t)$ and taking the time-average over the last eight tidal periods. The result is shown in Figure 2a: M1 crests are found all over the region where the downward directed M2 beam is present (see Figure 1b), implying that the M1-signal

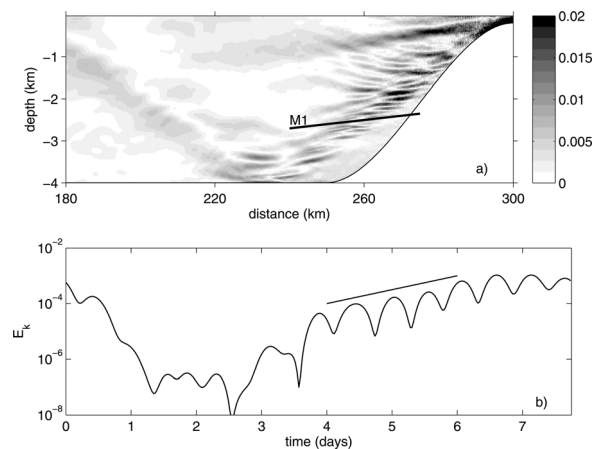


Figure 2. (a) Absolute u -component of the velocity field for M1-frequency motions averaged over the last 8 tidal periods of the computation, at latitude 27.5°N . (b) Kinetic energy of the M1-frequency motions versus time. The growth rate corresponding to the straight line is $1/(2.0 \text{ days})$.

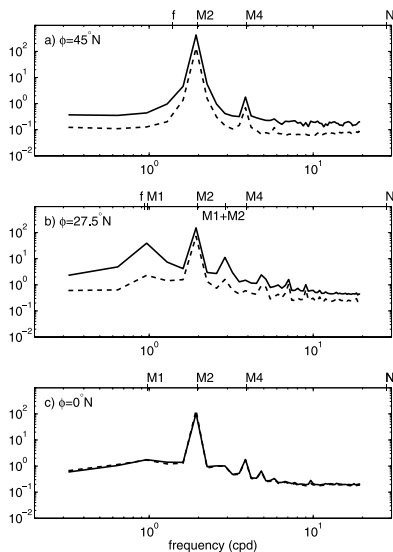


Figure 3. Solid lines represent spectra of kinetic energy density, defined as $E_k = \frac{1}{2}\rho_*(u^2 + v^2 + w^2)$, calculated by taking the average over the domain $x = 260\text{--}270$ km, from bottom to surface. (ρ_* is a constant reference value of density.) This represents the spectra over the slope, close to the area of generation, and before the M2 beam reflects at the bottom. Dashed lines show spectra of potential energy, defined in terms of temperature fluctuations.

indeed originates from the M2 beam. The growth rate associated with this subharmonic resonance is shown in Figure 2b. In the first few periods there is an M1-signal which is not related to subharmonic resonance, but rather to the transients in the system which starts from a state of rest. The transients disappear quickly, and after about three days an overall growth sets in. During this period of growth, the time needed to have an increase of the M1 kinetic energy by one order of magnitude is 2 days, which we define as the time scale characteristic of the growth, or inverse growth rate.

[15] Spectra of kinetic and potential energy-density are presented in Figure 3. In each run, they were calculated by taking the average over the spatial domain 260–270 km, using the last six tidal periods (i.e., 10–15). In Figure 3b a clear peak is present at the M1 frequency. Moreover, a smaller but significant peak is found at the frequency M1 + M2, which is probably due to a Doppler shift of the M1 signal by M2 currents. We note that peaks suggestive of either Doppler shifts or nonlinear interactions between near-inertial and tidal bands are often found in empirical spectra, too [e.g., Van Haren *et al.*, 2002]. The relatively short time span on which our spectra are based (6 M2 periods) implies that we cannot distinguish between the inertial frequency f and the slightly higher M1 in Figure 3b; however, the peak must be due to M1 since there is in our model no source for oscillations at f . At the equator (Figure 3c), a peak at M1 is still present, though much smaller than in Figure 3b. All in all, the spectra corroborate the idea that the M2 internal tide beam loses energy to M1 already soon after its generation, at all latitudes below the critical 28.8°N .

[16] In Figure 1 there is no visible sign of M1 ‘slices’ further away from the slope. This is confirmed in the spectra shown in Figure 4, which are based on the signal in the

‘open ocean’, in the interval $x = 200\text{--}210$ km, i.e., after bottom reflection of the M2 beam. In Figures 4b and 4c, no peak is found at M1. In principle, subharmonic resonance may also be at work in the reflected M2 beam, but since its amplitude is smaller, the timescale associated with this instability would be longer [e.g., Koudella and Staquet, 2006]. In fact, H. L. Simmons (The geography of subharmonic instability of the semi-diurnal internal tide, submitted to *Journal of Physical Oceanography*, 2005) found that there is a threshold which needs to be exceeded for the mechanism to work.

[17] The bottom reflection itself creates strong higher harmonics (M4, M6, etc.), which are visible in Figures 4a–4c. In contrast to an earlier study [Gerkema *et al.*, 2006], the higher harmonics are now not stronger at the equator than at mid-latitudes. Compared to that study, the horizontal resolution is now much higher, which improves the modelling of SR at low latitudes; the energy now lost to M1 at an early stage is no longer available to the creation of higher harmonics during reflection of the M2 beam.

4. Discussion

[18] Subharmonic resonance, as any other free instability, needs background ‘noise’ for the perturbation to exist in the first place. In our model runs, the forcing from an initial state of rest guarantees that a whole range of frequencies is present in the system, although of course M2 soon dominates. The presence of this background field, however weak, is instrumental in allowing instabilities to develop.

[19] The model results presented here are in good qualitative agreement with Carter and Gregg [2006]. Specifically, we found that the M2 internal tide beam loses already much of its energy to M1 over the continental slope, close to its generation region. The M1 signal manifests itself as near-horizontal slices in and beyond the M2 beam (Figures 1b and 1c).

[20] MacKinnon and Winters [2005] found that the M2 internal tide (in their case represented by the first mode

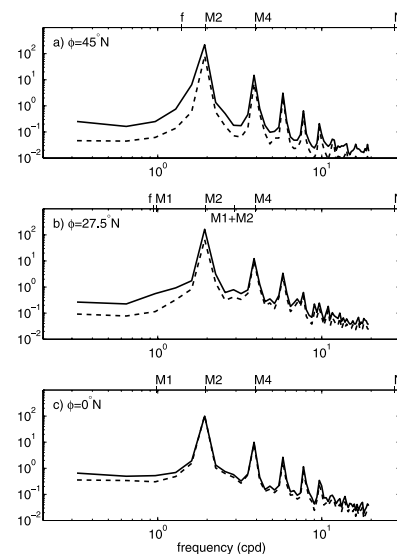


Figure 4. As in Figure 3, but now after bottom reflection of the M2 beam. (a–c) The signal in the domain $x = 200\text{--}210$ km is used.

only), starting at 15°N, propagates at first unperturbed northward; it is only in the range 22–29°N that a noticeable M1-signal is found (once a steady state is reached). In other words, their results suggest that SR is significant only in the vicinity of the critical latitude. Figure 3c, by contrast, shows that the occurrence extends to the equator if one includes many more modes, as is the case, implicitly, in our model runs. (It is indeed plausible that the higher modes, with their short vertical scales, should facilitate the transfer of energy to the M1 internal tides, which also have short vertical scales.) Figures 3b and 3c show that the M1-signal is larger near the critical latitude than at the equator. This can be explained by the fact that the group velocity of the M1 internal tide becomes smaller at higher latitudes, and indeed vanishes at the critical latitude. Near the critical latitude, then, the M1 internal tide stays within its source region (the M2 beam) and is therefore permanently fuelled. The growth rate associated with this instability was found to be 1/(2.0 days) (see Figure 2b). Thus, the timescale is shorter than that of 5 days as estimated by *MacKinnon and Winters* [2005].

[21] The computational cost of the calculations carried out here imposes a limit on the exploration of the parameter space, such as the dependence of Subharmonic Resonance, and the growth rate, on the various parameters in the system. However, we carried out additional calculations with weaker vertical and horizontal viscosity, and found no important changes; in particular, the resulting pattern of M1 slices (as shown in Figure 1b) remains similar.

[22] We finally note that the notion of a ‘critical’ latitude, in its common usage, is based on the requirement that the wave frequency (here M1) exceed $|f|$. This requirement, however, is modified when the horizontal component of the Coriolis vector is taken into account, since this slightly decreases the lowerbound of the range of allowable internal-wave frequencies [*LeBlond and Mysak*, 1978]. As a consequence, the critical latitude undergoes a poleward shift, and no longer coincides with the inertial latitude; this shift is particularly noticeable in the weakly stratified abyssal ocean, and can be as large as a few degrees [*Gerkema and Shrira*, 2005]. The dynamical consequences to SR are yet to be explored.

[23] **Acknowledgments.** We are much indebted to Jean-Michel Dupays (IDRIS, Paris) and Michael Schaferkötter for their help and suggestions which enabled us to get the MIT-GCM running in parallel.

We thank Annick Pichon and EPSHOM for supporting this work, under contract CA2003/01/CMO. The first author is financially supported by the NWO/ALW program CLIMA-DIM. The model runs were carried out on the supercomputers at IDRIS, under contract 040580 and 050580. We thank Hans van Haren for comments on an earlier version of this paper.

References

- Carter, G. S., and M. C. Gregg (2006), Persistent near-diurnal internal waves observed above a site of M2 barotropic-to-baroclinic conversion, *J. Phys. Oceanogr.*, in press.
- Gerkema, T., and V. I. Shrira (2005), Near-inertial waves on the “nontraditional” β plane, *J. Geophys. Res.*, *110*, C01003, doi:10.1029/2004JC002519.
- Gerkema, T., F. P. A. Lam, and L. R. M. Maas (2004), Internal tides in the Bay of Biscay: Conversion rates and seasonal effects, *Deep Sea Res., Part II*, *51*, 2995–3008, doi:10.1016/j.dsr2.2004.09.012.
- Gerkema, T., C. Staquet, and P. Bouruet-Aubertot (2006), Nonlinear effects in internal-tide beams, and mixing, *Ocean Modell.*, *12*, 302–318.
- Hibiya, T., and M. Nagasawa (2004), Latitudinal dependence of diapycnal diffusivity in the thermocline estimated using a finescale parameterization, *Geophys. Res. Lett.*, *31*, L01301, doi:10.1029/2003GL017998.
- Hibiya, T., M. Nagasawa, and Y. Niwa (2002), Nonlinear energy transfer within the oceanic internal wave spectrum at mid and high latitudes, *J. Geophys. Res.*, *107*(C11), 3207, doi:10.1029/2001JC001210.
- Koudella, C. R., and C. Staquet (2006), Instability mechanisms of a two-dimensional progressive internal gravity wave, *J. Fluid Mech.*, *548*, 165–195.
- LeBlond, P. H., and L. A. Mysak (1978), *Waves in the Ocean*, 602 pp., Elsevier, New York.
- MacKinnon, J. A., and K. B. Winters (2005), Subtropical catastrophe: Significant loss of low-mode tidal energy at 28.9°N, *Geophys. Res. Lett.*, *32*, L15605, doi:10.1029/2005GL023376.
- Marshall, J., C. Hill, L. Perelman, and A. Adcroft (1997), Hydrostatic, quasi-hydrostatic, and nonhydrostatic ocean modeling, *J. Geophys. Res.*, *102*, 5733–5752.
- Nagasawa, M., T. Hibiya, Y. Niwa, M. Watanabe, Y. Isoda, S. Takagi, and Y. Kamei (2002), Distribution of fine-scale shear in the deep waters of the North Pacific obtained using expendable current profilers, *J. Geophys. Res.*, *107*(C12), 3221, doi:10.1029/2002JC001376.
- Pingree, R. D., and A. L. New (1991), Abyssal penetration and bottom reflection of internal tidal energy in the Bay of Biscay, *J. Phys. Oceanogr.*, *21*(1), 28–39.
- Tabaï, A., T. R. Akylas, and K. G. Lamb (2005), Nonlinear effects in reflecting and colliding internal wave beams, *J. Fluid Mech.*, *526*, 217–243, doi:10.1017/S0022112004002769.
- Van Haren, H., L. Maas, and H. van Aken (2002), On the nature of internal wave spectra near a continental slope, *Geophys. Res. Lett.*, *29*(12), 1615, doi:10.1029/2001GL014341.

P. Bouruet-Aubertot, Laboratoire d’Océanographie et du Climat: Expérimentation et Approches Numériques, IPSL, 4 place Jussieu, F-75252 Paris, France.

T. Gerkema, Royal Netherlands Institute for Sea Research, P.O. Box 59, NL-1790 AB Den Burg, Texel, Netherlands. (gerk@nioz.nl)

C. Staquet, Laboratoire des Écoulements Géophysiques et Industriels, BP 53, F-38041 Grenoble, France.